

X-RAY BURST OSCILLATIONS: FROM FLAME SPREADING TO THE COOLING WAKE

SIMIN MAHMOODIFAR AND TOD STROHMAYER

Astrophysics Science Division and Joint Space-Science Institute, NASA's Goddard Space Flight Center, Greenbelt, MD 20771, USA

Draft version September 24, 2018

Abstract

Type I X-ray bursts are thermonuclear flashes observed from the surfaces of accreting neutron stars (NSs) in Low Mass X-ray Binaries. Oscillations have been observed during the rise and/or decay of some of these X-ray bursts. Those seen during the rise can be well explained by a spreading hot spot model, but large amplitude oscillations in the decay phase remain mysterious because of the absence of a clear-cut source of asymmetry. To date there have not been any quantitative studies that consistently track the oscillation amplitude both during the rise and decay (cooling tail) of bursts. Here we compute the light curves and amplitudes of oscillations in X-ray burst models that realistically account for both flame spreading and subsequent cooling. We present results for several such “cooling wake” models, a “canonical” cooling model where each patch on the NS surface heats and cools identically, or with a latitude-dependent cooling timescale set by the local effective gravity, and an “asymmetric” model where parts of the star cool at significantly different rates. We show that while the canonical cooling models can generate oscillations in the tails of bursts, they cannot easily produce the highest observed modulation amplitudes. Alternatively, a simple phenomenological model with asymmetric cooling can achieve higher amplitudes consistent with the observations.

Subject headings: stars: neutron — stars: oscillations — X-rays: binaries — X-rays: bursts

1. INTRODUCTION

Type I X-ray bursts are thermonuclear explosions observed from neutron stars (NSs) in many Low Mass X-ray Binaries (LMXBs). In these systems the NS accretes H- and/or He-rich matter from its companion star and when enough fuel is accumulated it can burn unstably causing periodic thermonuclear flashes on the NS surface (Strohmayer & Bildsten 2006; Galloway et al. 2008; Woosley & Taam 1976; Lamb & Lamb 1978). During a burst the X-ray flux rises by a factor of $\sim 10 - 20$ in a couple of seconds and then decays on a longer timescale as the surface cools. Oscillations have been detected during the rise and/or decay of some of these X-ray bursts with frequencies that are within a few Hz of the NS spin frequency (Strohmayer et al. 1996; Watts 2012). These “burst oscillations” are rotationally induced modulations resulting from an asymmetric temperature distribution on the NS surface. Their properties during the rise can be explained by a spreading hot spot that engulfs the star in about 1 s (Strohmayer et al. 1997; Chakraborty & Bhattacharyya 2014), however, oscillations observed during the decay phase (tail) of bursts have been harder to understand, as the source of asymmetry is less clear cut. Figure 1 shows an example of an X-ray burst observed with the *Rossi X-ray Timing Explorer (RXTE)* from the LMXB 4U 1728-34 on 1997 September 20, which shows oscillations both during burst rise and decay. As shown in the lower panel, during the rise the amplitude of the oscillations decreases until the peak of the burst, then it slowly increases in the tail until it reaches a maximum of $\approx 15\%$ and then decays again. Here and throughout we use the so-called half-amplitude (see §3 for a detailed explanation).

Several models have been proposed to explain the tail oscillations. It was suggested by Heyl (2004) that they

might be due to surface oscillation modes, such as r-modes (see also Lee & Strohmayer (2005)), however, it remains unclear whether the modes can be excited to the amplitudes required to account for the observed X-ray modulation amplitudes (see Figure 1), and estimates of their mode frequencies in the co-rotating frame are uncomfortably high to be consistent with the observed closeness of the burst oscillation and stellar spin frequencies (Berkhout & Levin 2008; Munro et al. 2002).

Alternatively, Cumming & Bildsten (2000) suggested that the tail oscillations might be due to a “cooling wake,” the temperature asymmetry due to cooling of the NS surface since it takes a finite time for both the atmosphere to cool and the burning to spread around the star. Spitkovsky et al. (2002) showed that the temperature gradient will drive a zonal thermal wind moving opposite to the NS rotation, and suggested that if an inhomogeneous feature such as a vortex were trapped in it, this could produce a flux modulation.

The timescale and geometry of the flame spreading are important, even for oscillations in the tail, because they set the “initial conditions” for subsequent cooling. Spitkovsky et al. (2002) first analyzed global hydrodynamical flows on an accreting NS and estimated the burning front speed taking into account the Coriolis effects. It was subsequently shown by Bhattacharyya & Strohmayer (2007) and Maurer & Watts (2008) that these effects are important for explaining observations of burst light curves and oscillation amplitudes (see also Chakraborty & Bhattacharyya (2014)). Spitkovsky et al. (2002) also argued that ignition is likely to start at the equator where the effective gravitational acceleration is lowest on a fast rotating NS, but later Cooper & Narayan (2007) showed that, depending on the accretion rate, ignition could occur on or off the equator. More recently, Cavecchi et al. in a series of papers (Cavecchi et al. 2013; Cavecchi

et al. 2015a,b) presented results of 2D hydrodynamical simulations of Type I X-ray bursts, including the effect of rotation and magnetic field which confirmed earlier results by Spitkovsky et al. (2002) regarding the importance of the Coriolis force on the flame propagation and showed that the magnetic field can also have an influence on the flame propagation and ignition location that, depending on the field strength, may be comparable to the Coriolis force.

However, to date there have not been any detailed, quantitative studies of the properties of tail oscillations that can be produced by realistic “cooling wake” models. Here, we attempt to address the question of whether such models can naturally account for the relatively large amplitudes seen in some bursts, or whether additional physical effects are needed. The plan of the paper is as follows. We first summarize our methods for modeling burst light curves, including ignition, spreading and subsequent cooling. We then present results for several models. First we explore two “canonical” cooling models, where each patch on the NS surface heats and cools in a prescribed way. In the first such model the heating and cooling functions are assumed to be identical for all parts of the star. In the second case we allow for latitude dependent variations in the cooling timescale, as might occur if the accretion rate (and thus column depth) were to vary with latitude. Such variations are expected for rapidly rotating stars due to latitudinal variations in the effective surface gravity (see Spitkovsky et al. (2002); Cooper & Narayan (2007)). We show that while such models do produce oscillations in the cooling tail, they cannot easily generate the large amplitudes seen in some bursts. Next, we explore a phenomenological “asymmetric” cooling model where parts of the star cool at significantly different rates. We show that this simple model can achieve higher amplitudes consistent with the largest observed. Finally, we briefly discuss several physical effects that could induce asymmetric cooling.

2. METHOD

To model X-ray burst light curves we assume the burst ignites a hot spot locally somewhere on the star and burning then spreads to engulf the entire surface. We assume that surface elements comprising the hot spot emit a black body spectrum, and we take into account in our computations both special- and general relativistic effects, including Doppler shifts and boosting, aberration, gravitational redshifts and light-bending in the Schwarzschild geometry (the so-called Schwarzschild+Doppler approximation, see Miller & Lamb (1998); Poutanen & Beloborodov (2006)). We also include an angle dependent emissivity in our models using an approximation from J. Poutanen (2012, private communication), where the spectrum is given by the Planck function, but the angular distribution is assumed to be that produced by a coherent electron scattering dominated, plane-parallel, semi-infinite atmosphere.

On a fast rotating NS the burning region is unlikely to spread uniformly over the surface and one needs to include the effect of the Coriolis force (Spitkovsky et al. 2002; Bhattacharyya & Strohmayer 2007; Maurer & Watts 2008). Spitkovsky et al. (2002) estimated the

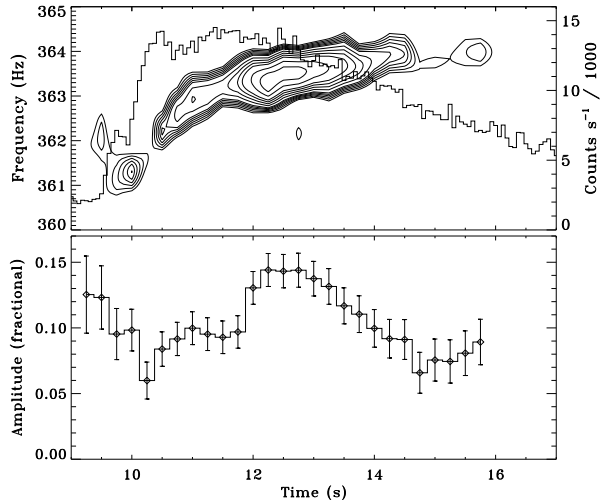


FIG. 1.— Dynamic power spectrum overplotted on the PCA light curve (top) for the 1997 September 20 burst from 4U 1728-34, and the fractional amplitude (half-amplitude, see Section 3) of oscillations during the burst (bottom). The contour levels that are plotted on the top panel are [20, 24, 28, 32, 36, 40, 50, 60, 70, 80, 100, 120]. Power spectra (and amplitudes) were computed from overlapping 1 s intervals, with a new interval starting every 1/4 s. The light curve has 1/16 s time bins.

flame speed in a NS ocean as follows:

$$v_{flame} \sim \left[\frac{gh_{hot}}{t_n} \frac{1/t_{fr} + \eta/t_n}{f^2 + (1/t_{fr} + \eta/t_n)^2} \right]^{1/2} \quad (1)$$

where t_n is the timescale of the thermonuclear burning which is set by the composition of the burning material, t_{fr} is the frictional coupling timescale between the top and bottom layers of the burning region, h_{hot} is the scale height of the ocean behind the burning front, $f = 2\Omega \cos \theta$ is the Coriolis parameter, where Ω is the angular spin frequency of the NS and θ is the colatitude of the spot center, and η is a constant of order unity.

When frictional coupling is weak, (i.e. $t_{fr} \gg t_n$ and $t_{fr} \gg 1/f$):

$$v_{flame} = \frac{v_{pole}}{\cos \theta} \quad (2)$$

where $v_{pole} \sim \sqrt{gh_{hot}/2\Omega t_n}$.

In the case of strong friction ($t_{fr} \lesssim t_n$ and $t_{fr} \ll 1/f$):

$$v_{flame} \sim \left(\frac{gh_{hot} t_{fr}}{t_n} \right)^{1/2} \quad (3)$$

The flame speed reaches its maximum value in the intermediate regime when friction is important (i.e. $t_{fr} \lesssim t_n$ and $t_{fr} = 1/f$):

$$v_{flame} = \frac{v'_{pole}}{\sqrt{\cos \theta}} \quad (4)$$

where $v'_{pole} \sim \sqrt{gh_{hot}/(4\Omega t_n)}$.

Cavecchi et al. (2013) performed hydrodynamic simulations of the lateral propagation of a deflagrating, vertically resolved flame on the surface of a rotating, accreting NS and showed that the horizontal propagation velocity is proportional to $\frac{1}{\cos \theta}$. In our modeling we consider both cases of $1/\cos \theta$ and $1/\sqrt{\cos \theta}$ for the latitude dependence of the flame speed. We consider flame speeds such that

the time to ignite the entire stellar surface is less than a few seconds, so as to approximately match the observed rise times of bursts.

We consider several models to explore the properties of burst oscillations in the tail. The first is a “canonical” cooling model in which we assume that, once ignited, all surface elements of the star follow the same temperature evolution (we refer to this as the “symmetric” cooling model). In this model each surface element, once ignited, evolves in temperature according to an exponential rise and decay. We use an expression similar to Bhattacharyya & Strohmayer (2006a) and Maurer & Watts (2008) for the temperature evolution:

$$\begin{aligned}
 T &= T_0, & t &\leq t_{ig} \\
 &= (T_0 + \Delta T[1 - \exp(\frac{-(t - t_{ig})}{\tau_r})]), & t_{ig} &\leq t \leq t_{ig} + \Delta t_r \\
 &= (T_0 + \Delta T_m \exp(\frac{-(t - (t_{ig} + \Delta t_r))}{\tau_d})), & t &\geq t_{ig} + \Delta t_r
 \end{aligned} \tag{5}$$

where t_{ig} , Δt_r , τ_r , τ_d are the ignition time, the temperature rise time (from ignition to peak), the rise timescale, and the decay timescale, respectively. In addition, T_0 and ΔT are the background (minimum) temperature and temperature contrast, respectively and $\Delta T_m = \Delta T[1 - \exp(\frac{-\Delta t_r}{\tau_r})]$.

1D hydro simulations of X-ray bursts (Taam 1980; Woosley et al. 2004; Weinberg et al. 2006) give the light curve for a single patch on the star. The shape of the light curve in these models is sensitive to the composition of the accreted layer and the burning regime. The temperature profile that we use here gives a reasonable approximation to the shape of a single patch light curve in these simulations. Temperature parameters used in our models are $T_0 = 1.5$ keV, $\Delta T = 1.5$ keV, $\Delta t_r = 0.46$ s, $\tau_r = 0.1$ s and $\tau_d = 6$ s. These parameters result in a burst rise time of about 1 s and a decay time of about 11 s. Since there is a finite time over which the burning spreads, there will always be some temperature gradient across the NS surface. This temperature asymmetry combined with rotation of the star results in oscillations during the burst tail.

We also consider a variation of the “symmetric” model in which the cooling timescale, τ_d , is assumed to vary with latitude (we call this the “latitude-dependent” cooling model). On a rapidly rotating NS the effective gravitational acceleration is reduced along the rotational equator and enhanced at the poles. This can lead to variations in the local accretion rate and hence the accreted column with latitude (Cooper & Narayan 2007). Since the vertical cooling time is basically set by the column depth at which heat is released, coupled with the thermal conductivity of the material above, variations in the accreted column and/or composition across the star could in principle lead to changes in the cooling timescale with latitude. Since the local mass accretion rate is proportional to the inverse of the effective gravitational acceleration ($\dot{m}(\theta) \propto g_{eff}^{-1}(\theta)$) (Spitkovsky et al. 2002; Cooper & Narayan 2007), we assume that the cooling (decay) timescale, τ_d , in Eq. 5 varies with latitude like $1/g_{eff}(\theta) \propto 1/(1 + c_e \bar{\Omega}^2 \sin^2 \theta + c_p \bar{\Omega}^2 \cos^2 \theta)$. Where

$c_e = -0.791 + 0.776(M/R)$, $c_p = 1.138 - 1.431(M/R)$ and $\bar{\Omega} = \Omega \sqrt{R^3/M}$ (in geometric units $G = c = 1$; Al-Gendy & Morsink (2014)). Note that g_{eff} is lowest at the equator and increases toward the pole, and therefore the mass accretion rate and the cooling timescale are largest at the equator and decrease toward the poles. While this model includes variations in the cooling timescale across the star, the variations retain symmetry about the spin axis.

Lastly, we consider a simple phenomenological model with “asymmetric” cooling. By this we mean that the variations in the cooling timescale are no longer symmetric about the rotational axis. In this model we do not consider the full temperature evolution of each individual surface element. In this “spreading cooling wake” model we have only two temperatures, T_h and T_c that represent the temperature of the burning region and the rest of the star (cool regions), respectively. In this model, when burning spreads over the star, the temperature of each patch changes from T_c to T_h . The burning spreads in the same way as in the previous model, the only difference is that at $t = t_{rise} = 1$ s when the whole surface is burning there is no temperature gradient across the star. When cooling begins, regions that started burning earlier are assumed to cool first and their temperature changes from T_h to T_c . The cooling is assumed to spread in the exact same way as the burning but just over a longer time. Here, we use a total duration of 10 s for the cooling phase, which is characteristic of observed bursts. That is, the speed of the spreading of cooling is taken to be $0.1 \times v_{flame}$, which gives a total decay time of 10 s. In this model at $t = 1$ s all patches on the surface are ignited and have a temperature of T_h , but since the cooling duration is longer, and also the cooling is assumed to spread in a similar way as burning, the patches that burned first will cool first and also in a shorter time than other parts of the star. For example, at $t = 1.5$ s a small region on the surface that has been ignited first will be already cool (with $T = T_c$), but it will take longer (up to 10 s) for the patches that burned last to cool. Therefore the total time that a given patch is hot is different from any other patch. For example, the total time that the first burned patch is hot is about 1 s, the patch that burned at $t = 0.5$ s will be hot for ~ 5.5 s and the last patch that burned at $t = 1$ s will be hot for ~ 10 s. This simple model approximates what may happen if the timescale of cooling varies across the surface in a manner that breaks the symmetry about the rotation axis, i.e. if the heat transport varies with position on the star. For example, if there is significant transverse heat flow between hot and cold regions then the timescale of cooling in the area where burning started first might be shorter since it is initially surrounded by cooler regions, but those that burn last are already surrounded by hot areas and therefore it might take longer for them to cool. While it is likely that lateral conductive heat transport is negligible given the large difference between the vertical and horizontal scales in the burning front (Cavecchi et al. 2013), convective and hydrodynamic flows not fully captured by 2D hydrodynamic simulations could perhaps increase the transverse heat flow. Other possibilities for inducing asymmetric cooling would be different fuel depths or composition across the star and also varying amounts of

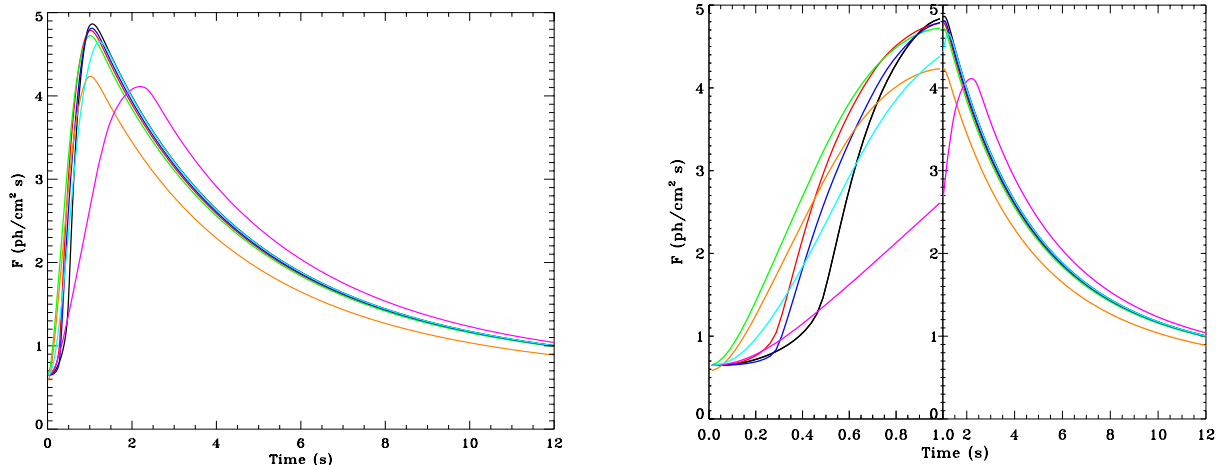


FIG. 2.— Bolometric light curves for the “symmetric” cooling model. The left panel shows the smoothed bolometric light curves during the rise and decay of the burst (averaged over five rotation cycles). The right panel is similar to the left panel, but the first second of the light curve (burst rise) is shown on an expanded scale. The black, red, green and blue curves correspond to models with $M = 1.4M_{\odot}$, $R=10$ km, $\nu=400$ Hz, $i = 70^{\circ}$, $D = 10$ kpc and $v_{flame} \propto \frac{1}{\cos \theta}$ with $\theta_s = 10, 30, 85$ and 150° respectively. The orange and cyan curves have similar parameters as the green curve ($\theta_s = 85^{\circ}$) but with $M = 1.8M_{\odot}$ and $v_{flame} \propto \frac{1}{\sqrt{\cos \theta}}$ respectively. The magenta model is the same as the cyan one but with a spreading speed that is half of that model. Temperature parameters used in these models are $T_0 = 1.5$ keV, $\Delta T = 1.5$ keV, $\Delta t_r = 0.46$ s, $\tau_r = 0.1$ s and $\tau_d = 6$ s.

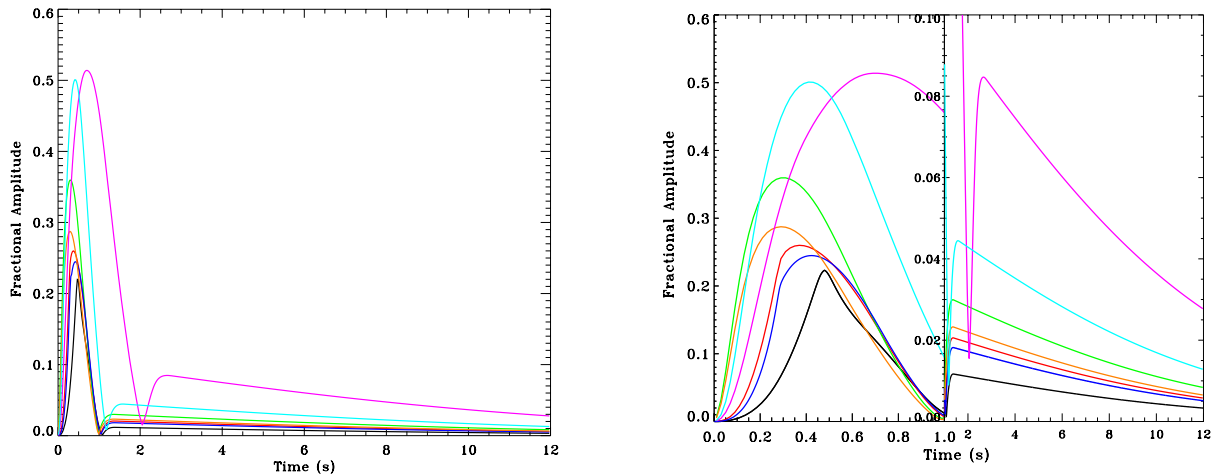


FIG. 3.— Fractional oscillation amplitude vs. time for the “symmetric” cooling model. The color coding is the same as Figure 2. On the right panel the fractional amplitudes are shown on an expanded scale up to $t = 1$ s. Note that the vertical scales are also different before and after $t = 1$ s.

heat flux from deeper layers for different parts of the NS surface.

3. RESULTS

Figure 2 shows several burst light curves computed with the canonical (“symmetric”) cooling model. Different curves correspond to different ignition latitudes, θ_s , NS compactness and flame spreading speeds ($v_{flame} \propto \frac{1}{\cos \theta}$ and $\frac{1}{\sqrt{\cos \theta}}$). The black, red, green and blue curves correspond to models with $M = 1.4M_{\odot}$, $R = 10$ km, $\nu = 400$ Hz, $i = 70^{\circ}$, $D = 10$ kpc and $v_{flame} \propto \frac{1}{\cos \theta}$ with $\theta_s = 10, 30, 85$ and 150° , respectively. Here, M , R , ν , i

and D are the stellar mass, radius, spin frequency, observer’s inclination angle, and the distance to the source, respectively. The orange and cyan curves have similar parameters as the green curve (all have $\theta_s = 85^{\circ}$ but with $M = 1.8M_{\odot}$ and $v_{flame} \propto \frac{1}{\sqrt{\cos \theta}}$, respectively, to show the effect of compactness and flame spreading velocity on the light curve. The magenta curve has the same parameters as the cyan curve but with a spreading speed that is half of the cyan one.

To highlight the differences in the rising phase more clearly, in Figure 2 (right panel) we also show the light curves on an expanded scale up to $t = 1$ s. As burning

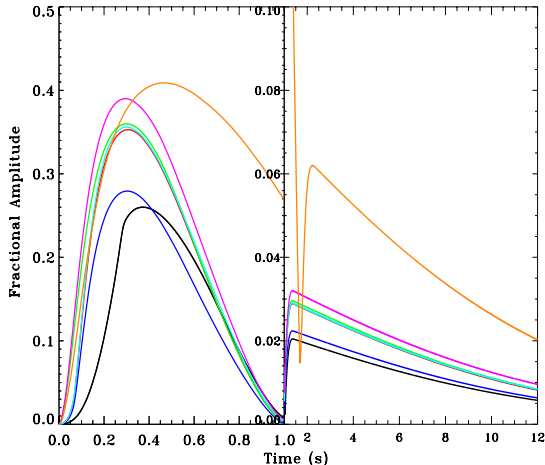


FIG. 4.— Fractional amplitudes for the “canonical” cooling model with latitude-dependent cooling timescales. The black, red, and green curves correspond to models with $M = 1.4M_{\odot}$, $R=10$ km, $\nu=400$ Hz, $i = 70^{\circ}$, $D = 10$ kpc and $v_{flame} \propto \frac{1}{\cos\theta}$ with $\theta_s = 30, 60$, and 85° respectively. The blue and cyan curves are the same as the red one but with $M = 1.8M_{\odot}$ and $\nu=600$ Hz, respectively (note that red, cyan and green curves almost overlap). The magenta curve has $M = 1.4M_{\odot}$, $\theta_s = 85^{\circ}$, $\nu=600$ Hz and $R=12$ km. The orange curve has similar parameters as the magenta one, but with a spreading speed that is half of that model. Note that the amplitudes are shown on an expanded scale up to $t = 1$ s. Also the vertical scale is different before and after $t = 1$ s on this plot.

spreads over the surface the flux increases until it engulfs the whole star, after that, since the temperature of each surface element decays exponentially with time, the flux decreases. The shape of the light curve during the rising phase depends on several factors such as the ignition latitude, the flame spreading geometry and speed, and its latitudinal dependence (Maurer & Watts 2008). When ignition starts near a pole (black, red and blue curves with $\theta_s = 10, 30$ and 150°) the rise light curve is more concave (rises more slowly) compared to when it starts near the equator ($\theta_s = 85^{\circ}$, see Maurer & Watts (2008)).

Figure 3 shows the evolution of burst oscillation amplitudes during the burst rise and decay for the “symmetric” model. The color coding is similar to Figure 2. To compute the fractional amplitudes we calculate the so-called half-amplitude. The light curve is phase-folded in the time intervals of interest, and the amplitude is determined as $f = (I_{max} - I_{min}) / (I_{max} + I_{min})$, where I_{max} and I_{min} are the maximum and minimum values in the phase-folded light curves, respectively. To the extent that the light curves are consistent with sinusoids, this is equivalent to fitting the phase-folded light curve with the model $A + B \sin(2\pi\nu t + \phi_0)$, and defining the fractional amplitude as B/A . This definition of fractional amplitude is $\sqrt{2}$ times larger than the rms amplitude used in many papers. Therefore, to compare the rms amplitudes with our amplitudes, they should be multiplied by $\sqrt{2}$.

The maximum of the tail amplitudes in the “symmetric” model ranges from 1.5% to 8% depending on the ignition latitude, NS compactness and the flame spreading geometry/speed. The temperature asymmetry combined with rotation of the star produces oscillations during the decaying phase, but since the temperature gra-

dient across the surface is not very large after burning has spread over the whole surface, the amplitude does not get large enough to explain the observations where the amplitudes in the tail can be $\geq 15\%$ (see Figure 1; Galloway et al. (2008); Muno et al. (2002); van Straaten et al. (2001)). Note that the amplitudes only slightly increase by increasing ΔT in Eq. 5. The largest tail amplitude is produced by the model with the longest (slowest) rise-time (spreading speed). This is not too surprising since there is a longer time for cooling to introduce a temperature gradient when the spreading speed is slower (assuming a constant cooling timescale). However, some bursts with large tail amplitudes have fast (≈ 1 s) rises (see Figure 1), so this effect cannot account for all large observed tail amplitudes.

In Figure 4 we show the evolution of the fractional amplitudes for several models with latitude-dependent cooling timescales. The black, red, and green curves correspond to models with $M = 1.4M_{\odot}$, $R=10$ km, $\nu=400$ Hz, $i = 70^{\circ}$, $D = 10$ kpc, $v_{flame} \propto \frac{1}{\cos\theta}$ and $\theta_s = 30, 60$, and 85° , respectively. The blue and cyan curves are the same as the red one but with $M = 1.8M_{\odot}$ and $\nu=600$ Hz, respectively. The magenta curve has $M = 1.4M_{\odot}$, $\theta_s = 85^{\circ}$, $\nu=600$ Hz and $R=12$ km, and the orange model has similar parameters to the magenta one, but with a spreading speed that is half of that model. Increasing both the spin frequency and stellar radius increases the variations in effective gravitational acceleration from equator to pole, thus making the difference between cooling timescales at the equator and pole larger. This causes a larger temperature asymmetry across the star and leads to somewhat larger fractional amplitudes. Comparing the red and cyan curves, which almost overlap, and also the green and magenta curves we note that increasing the frequency has a smaller effect on increasing the amplitudes than the radius. However, comparing Figure 4 with Figure 3 we see that the fractional amplitudes in the burst tail only slightly increase with the inclusion of a latitude-dependent cooling timescale, thus, this model is still not able to explain the largest observed amplitudes in burst tails.

Figure 5 shows the light curves for the phenomenological model with “asymmetric” cooling. The black, red, green and blue curves correspond to models with $M = 1.4M_{\odot}$, $R=10$ km, $\nu=400$ Hz, $i = 70^{\circ}$, $D = 10$ kpc, $T_h = 3$ keV, $\Delta T = T_h - T_c = 1.5$ keV and $v_{flame} \propto \frac{1}{\cos\theta}$ with $\theta_s = 10, 30, 85$ and 150° respectively. The orange, magenta and cyan curves are similar to the green curve ($\theta_s = 85^{\circ}$) but with $M = 1.8M_{\odot}$, $\Delta T=2$ keV and $v_{flame} \propto \frac{1}{\sqrt{\cos\theta}}$, respectively. As for the “symmetric” model, one can see a clear difference in the shape of the light curves during the rising phase depending on whether the ignition starts near the pole or the equator (Maurer & Watts 2008). Also, for models where ignition starts near the pole the light curve decays more slowly in the first few seconds after the peak compared with near-equatorial ignition. This is due to our assumption for this model that cooling spreads in the same way as burning (i.e., with the same angular dependence as from the Coriolis effects), in which case it would take longer for the cooling to reach the equator.

Figure 6 shows the fractional amplitudes during the burst rise and decay for the “asymmetric” cooling model.

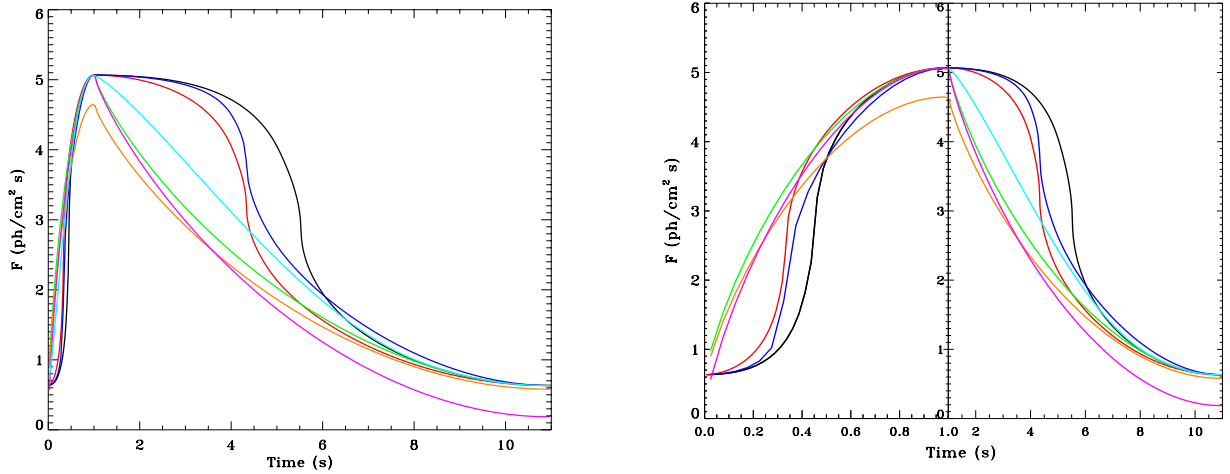


FIG. 5.— Left panel shows the smoothed bolometric light curves for the rise and decay of the burst in our “asymmetric” cooling model. The black, red, green and blue curves correspond to models with $M = 1.4M_{\odot}$, $R=10$ km, $\nu=400$ Hz, $i = 70^{\circ}$, $D = 10$ kpc, $T_h = 3$ keV, $\Delta T = T_h - T_c = 1.5$ keV and $v_{flame} \propto \frac{1}{\cos \theta}$ with $\theta_s = 10, 30, 85$ and 150° respectively. The orange, magenta and cyan curves are similar to the green curve ($\theta_s = 85^{\circ}$) but with $M = 1.8M_{\odot}$, $\Delta T=2$ keV and $v_{flame} \propto \frac{1}{\sqrt{\cos \theta}}$ respectively. Right panel shows the light curves on an expanded scale up to $t = 1$ s (burst rise).

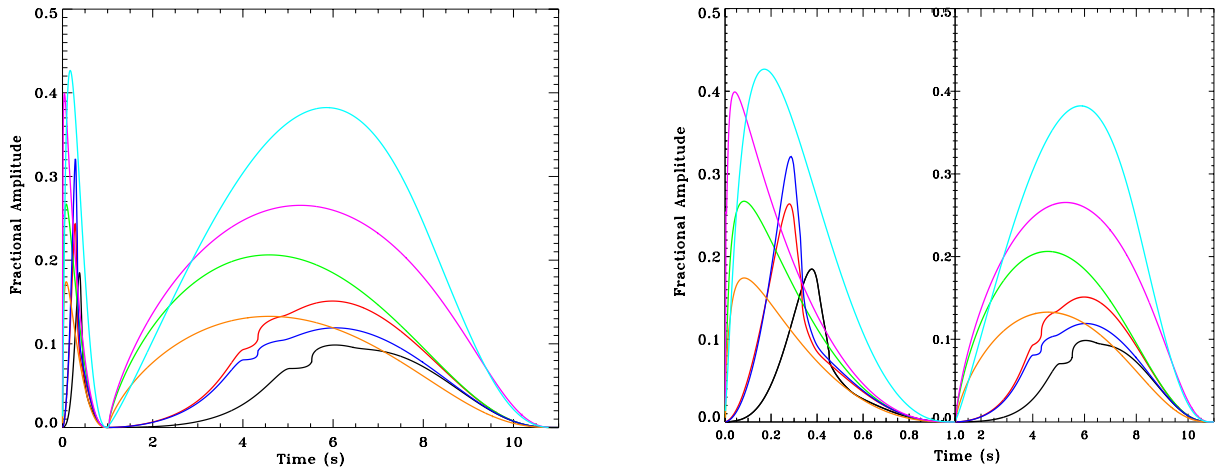


FIG. 6.— Fractional oscillation amplitude vs. time for the “asymmetric” cooling model. The color coding is the same as Figure 5. In the right panel the fractional amplitudes are shown on an expanded scale up to $t = 1$ s.

The color coding is similar to Figure 5. During the burst rise as the hot spot gets larger, the fractional amplitude increases, until burning reaches the equatorial region and quickly wraps around the equator due to the Coriolis effect. This then results in more symmetric burning and therefore smaller fractional amplitudes. As the burning spreads over a larger portion of the star and also the total flux increases the fractional amplitude continues to decrease. When burning engulfs the whole star there is by assumption no longer any temperature asymmetry in this model and the fractional amplitude goes to zero.¹ After that, as the star begins to cool, the temper-

ature asymmetry and therefore the fractional oscillation amplitude grows. The amplitude of the tail oscillations can be significantly larger in this model compared to the “canonical” models, and ranges from less than 10% to about 35% depending on the compactness of the star, the temperature gradient and the flame spreading speed in this model. The sudden rise in amplitudes around $t = 4 - 6$ s in the red, blue and black curves is due to

the temperature changes like a step function as opposed to the gradual temperature change in the “canonical” models where there is always some temperature difference between different regions, even in the peak of the burst. If there was a gradual change from T_c to T_h and vice versa, the amplitude would not go to zero at the peak.

¹ This is due to the simplification in the asymmetric model where

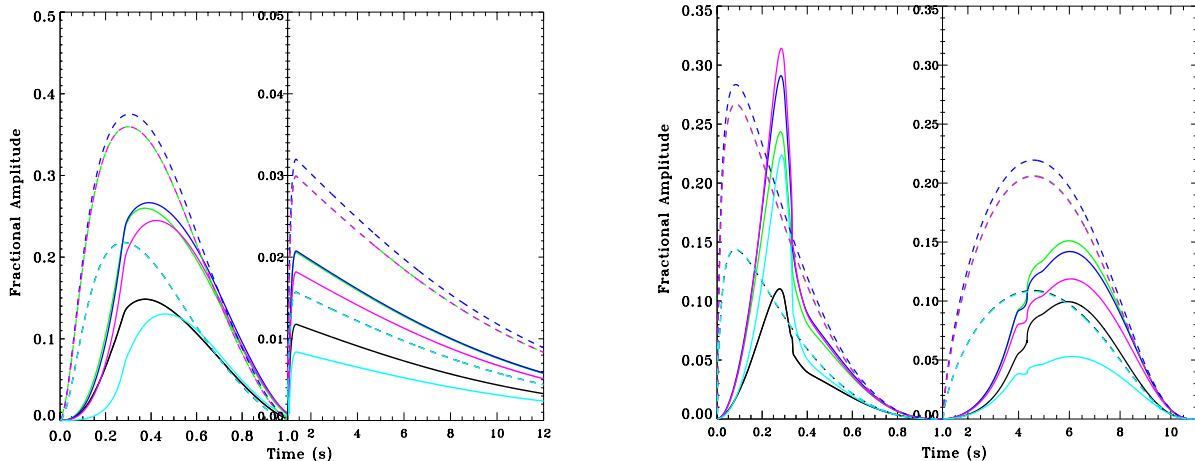


FIG. 7.— Fractional amplitude vs. time for different inclination angles for the “symmetric” cooling model (left panel) and “asymmetric” model (right panel). In both plots the solid curves correspond to an ignition latitude of $\theta_s = 30^\circ$ and the dashed curves correspond to an ignition latitude of $\theta_s = 85^\circ$. The black, green, blue, magenta and cyan curves correspond to $i = 30, 70, 90, 110$ and 130° , respectively. Other parameters are the same as those used for the red and green models in Figures 2 and 4. Note that the amplitudes are shown on an expanded scale up to $t = 1$ s. Also the vertical scale is different before and after $t = 1$ s on the left panel.

the rapid cooling near the equator, and therefore a sudden decrease in the total flux. This is because when the cooling front reaches the equator it spreads around the star and decreases the total flux, but since the spreading is more or less symmetric around the equator it doesn’t cause a big temperature asymmetry, therefore the amplitude of the oscillations stays approximately the same, but since the total flux decreases, the fractional amplitude increases at that point. In general the amplitude of the tail oscillations are larger when $v_{flame} \propto \frac{1}{\sqrt{\cos \theta}}$ compared to $v_{flame} \propto \frac{1}{\cos \theta}$, assuming that the burning engulfs the star in ~ 1 s in both cases. The reason is that in the former case it takes longer for the burning to spread around the equator and therefore there will be more temperature asymmetry compared to the latter. We also note that as the compactness of the star increases the oscillation amplitudes decrease, since at each time a larger portion of the surface would be visible.

Since we are interested in exploring the largest amplitudes that can be produced in the cooling tails of bursts we used a favorable observer’s inclination angle of 70° for the results shown in Figures 2 - 6. However, for completeness, in Figure 7 we also explored the effect of inclination angle on the amplitude of burst oscillations. The left panel in this figure corresponds to the “symmetric” cooling model, and the right panel to the “asymmetric” model. In both plots the solid and dashed curves correspond to an ignition latitude of $\theta_s = 30$ and 85° , respectively. The black, green, blue, magenta and cyan curves represent $i = 30, 70, 90, 110$ and 130° , respectively, with $M = 1.4M_\odot$, $R = 10$ km, $\nu = 400$ Hz, $D = 10$ kpc, $v_{flame} \propto \frac{1}{\cos \theta}$ and $\Delta T = 1.5$ keV. In the “symmetric” model the oscillation amplitudes increase as the inclination angle gets closer to 90° , where at each time more temperature asymmetry would be observable. In the cases where the ignition starts near the equator there is a symmetry between inclination angles above and below the equator. For example, for $\theta_s = 85^\circ$, the

amplitudes are almost the same for $i = 70^\circ$ and 110° and for $i = 30^\circ$ and 130° . We note that such symmetry doesn’t exist when the ignition starts off the equator. In the “asymmetric” model the effect of the inclination angle on oscillation amplitudes are similar to the “symmetric” model for the cases where the ignition starts near the equator, but for off-equatorial ignitions, $i = 90^\circ$ no longer corresponds to the highest amplitudes.

4. SUMMARY AND CONCLUSIONS

In this paper we have computed for the first time the light curves and amplitudes of oscillations in X-ray burst models that realistically account for both flame spreading and subsequent cooling. This allows us to consistently track the oscillation amplitude both during the rise and decay (tail) in these models. We have compared results from several models. We consider two variations of “canonical” cooling models, one “symmetric” model in which each patch on the NS heats and cools in the same manner, and another which allows for variations in the cooling timescale with latitude, as could result from rotationally induced changes in the effective gravity. We also explored a simple “asymmetric” model where parts of the star that ignite first cool faster than those that burn last. This may happen, for example, if there is significant transverse heat exchange between hot and cold regions, or if the local cooling time is shorter near the ignition site than elsewhere on the star. We showed that the “canonical” cooling models can generate oscillations in the tails of bursts, but they cannot easily produce the highest observed modulation amplitudes. One way to increase the modulation amplitudes in such models is to increase the temperature contrast during the burst. For a fixed cooling timescale this can be done by decreasing the flame speed (increasing the rise time), but to reach substantially higher amplitudes one requires rise times longer than typically observed. Nevertheless, a signature of such a “canonical” cooling wake would be a positive correlation between burst rise time

and tail oscillation amplitude. Another way to increase the modulation amplitudes in the “canonical” model is to include a latitude-dependent cooling timescale in the temperature evolution. We showed in Figure 4 that although this will boost the amplitudes, it is still not large enough to explain the observed amplitudes in some of the burst tails.

On the other hand, a relatively simple phenomenological model with asymmetric cooling, where the speed of the cooling wake is different in different regions on the star, and is not symmetric about the rotation axis, can achieve higher amplitudes consistent with the highest observed. While the particular asymmetric model we employ is not rigorously self-consistent, and it may tend to overestimate actual cooling asymmetries, its results demonstrate that asymmetric cooling processes can boost the amplitude of tail oscillations, and are thus important areas for further research. Indeed, the amplitude evolutions of several of the models in Figure 6 have some qualitative similarities to that of the 4U 1728-34 burst shown in Figure 1, in particular the rise in amplitude several seconds after the peak.

A number of physical effects could plausibly lead to asymmetric cooling, and we briefly discuss several here. As we noted previously, significant transverse heat flow could lead to such asymmetries. The ignition site is ini-

tially surrounded by cooler regions, thus, heat flow laterally away from the hot spot could cool it faster than regions which are last to burn, since they are surrounded by hot, already ignited fuel. Previous work has shown that the vertical scale height within the front is much smaller than the relevant transverse length scales (for example, the Rossby adjustment radius, Spitkovsky et al. 2002; Cavecchi et al. 2013). This suggests that thermal conduction is unlikely to result in significant transverse heat flow. However, 2D simulations indicate that larger scale horizontal (zonal) and convective flows can be set-up by the burning. These flows could perhaps transport heat in a manner which induces some level of asymmetric cooling like that present in our simple “asymmetric” model. Fully 3D hydrodynamic simulations will likely be needed to further explore the likely magnitude of any such effects, and they can then be incorporated into fully self consistent light curve models.

We would like to thank Cole Miller and the anonymous referee for helpful comments. SM’s research was supported by an appointment to the NASA Postdoctoral Program at the GSFC. This material is based upon work supported by the National Aeronautics and Space Administration under Grant No. 14-ADAP14-0198 issued through the Science Mission Directorate.

REFERENCES

- AlGendy, M., & Morsink, S. M. 2014, *ApJ*, 791, 78
 Berkhout, R. G., & Levin, Y. 2008, *MNRAS*, 385, 1029
 Bhattacharyya, S., & Strohmayer, T. E. 2006a, *ApJ*, 636, L121
 —. 2006b, *ApJ*, 642, L161
 —. 2007, *ApJ*, 666, L85
 Cavecchi, Y., Watts, A. L., Braithwaite, J., & Levin, Y. 2013, *MNRAS*, 434, 3526
 Cavecchi, Y., Watts, A. L., Levin, Y., & Braithwaite, J. 2015a, *MNRAS*, 448, 445
 Cavecchi, Y., Levin, Y., Watts, A. L., & Braithwaite, J. 2015b, *arXiv:1509.02497*
 Chakraborty, M., & Bhattacharyya, S. 2014, *ApJ*, 792, 4
 Cooper, R. L., & Narayan, R. 2007, *ApJ*, 657, L29
 Cumming, A., & Bildsten, L. 2000, *ApJ*, 544, 453
 Galloway, D. K., Muno, M. P., Hartman, J. M., Psaltis, D., & Chakraborty, D. 2008, *ApJS*, 179, 360
 Heyl, J. S. 2004, *ApJ*, 600, 939
 Lamb, D. Q., & Lamb, F. K. 1978, *ApJ*, 220, 291
 Lee, U., & Strohmayer, T. E. 2005, *MNRAS*, 361, 659
 Maurer, I., & Watts, A. L. 2008, *MNRAS*, 383, 387
 Miller, M. C., & Lamb, F. K. 1998, *ApJ*, 499, L37
 Muno, M. P., Chakraborty, D., Galloway, D. K., & Psaltis, D. 2002, *ApJ*, 580, 1048
 Muno, M. P., Özel, F., & Chakraborty, D. 2002, *ApJ*, 581, 550
 Piro, A. L., & Bildsten, L. 2005, *ApJ*, 629, 438
 Poutanen, J., private communication (LOFT Dense Matter working group)
 Poutanen, J., & Beloborodov, A. M. 2006, *MNRAS*, 373, 836
 Spitkovsky, A., Levin, Y., & Ushomirsky, G. 2002, *ApJ*, 566, 1018
 Strohmayer, T., & Bildsten, L. 2006, *New views of thermonuclear bursts*, ed. W. H. G. Lewin & M. van der Klis, 113–156
 Strohmayer, T. E., Zhang, W., & Swank, J. H. 1997, *ApJ*, 487, L77
 Strohmayer, T. E., Zhang, W., Swank, J. H., et al. 1996, *ApJ*, 469, L9
 Taam, R. E. 1980, *ApJ*, 241, 358
 van Straaten, S., van der Klis, M., Kuulkers, E., & Méndez, M. 2001, *ApJ*, 551, 907
 Watts, A. L. 2012, *ARA&A*, 50, 609
 Weinberg, N. N., Bildsten, L., & Schatz, H. 2006, *ApJ*, 639, 1018
 Woosley, S. E., & Taam, R. E. 1976, *Nature*, 263, 101
 Woosley, S. E., Heger, A., Cumming, A., et al. 2004, *ApJS*, 151, 75